Radiology: Cardiothoracic Imaging

ORIGINAL RESEARCH

Cardiac Virtual Noncontrast Images for Calcium Quantification with Photon-counting Detector CT

Victor Mergen, MD • Sadaf Ghouse, BMed • Thomas Sartoretti, BMed • Robert Manka, MD • André Euler, MD • Albert M. Kasel, MD • Hatem Alkadhi, MD, MPH, EBCR • Matthias Eberhard, MD, EBCR

From the Institute of Diagnostic and Interventional Radiology (V.M., S.G., T.S., R.M., A.E., H.A., M.E.) and Department of Cardiology, University Heart Center (R.M., A.M.K.), University Hospital Zurich, University of Zurich, Raemistrasse 100, CH-8091, Zurich, Switzerland; and Institute of Radiology, Spitäler fmi AG, Unterseen, Switzerland (M.E.). Received December 9, 2022; revision requested January 12, 2023; revision received March 29; accepted May 8. **Address correspondence to** M.E. (email: *matthias.eberhard@usz.ch*).

Authors declared no funding for this work.

Conflicts of interest are listed at the end of this article.

Radiology: Cardiothoracic Imaging 2023; 5(3):e220307 • https://doi.org/10.1148/ryct.220307 • Content codes: CA CT

Purpose: To assess the accuracy of aortic valve calcium (AVC), mitral annular calcium (MAC), and coronary artery calcium (CAC) quantification and risk stratification using virtual noncontrast (VNC) images from late enhancement photon-counting detector CT as compared with true noncontrast images.

Materials and Methods: This retrospective, institutional review board–approved study evaluated patients undergoing photon-counting detector CT between January and September 2022. VNC images were reconstructed from late enhancement cardiac scans at 60, 70, 80, and 90 keV using quantum iterative reconstruction (QIR) strengths of 2–4. AVC, MAC, and CAC were quantified on VNC images and compared with quantification of AVC, MAC, and CAC on true noncontrast images using Bland-Altman analyses, regression models, intraclass correlation coefficients (ICC), and Wilcoxon tests. Agreement between severe aortic stenosis likelihood categories and CAC risk categories determined from VNC and true noncontrast images was assessed by weighted κ analysis.

Results: Ninety patients were included (mean age, 80 years ± 8 [SD]; 49 male patients). Scores were similar on true noncontrast images and VNC images at 80 keV for AVC and MAC, regardless of QIR strengths, and VNC images at 70 keV with QIR 4 for CAC (all $P > .05$). The best results were achieved using VNC images at 80 keV with QIR 4 for AVC (mean difference, 3; ICC = 0.992; $r = 0.98$) and MAC (mean difference, 6; ICC = 0.998; $r = 0.99$), and VNC images at 70 keV with QIR 4 for CAC (mean difference, 28; ICC = 0.996; $r = 0.99$). Agreement between calcification categories was excellent on VNC images at 80 keV for AVC (κ = 0.974) and on VNC images at 70 keV for CAC (κ = 0.967).

Conclusion: VNC images from cardiac photon-counting detector CT enables patient risk stratification and accurate quantification of AVC, MAC, and CAC.

Supplemental material is available for this article.

Patients with severe, degenerative aortic stenosis have a high prevalence and extent of aortic valve, mitral annular, and coronary artery calcifications (1) which can be accurately quantified with noncontrast cardiac CT (2). The aortic valve calcium (AVC) score quantifies the calcium burden of the aortic valve, provides a complementary tool for the assessment of severe aortic stenosis in patients with inconclusive echocardiographic findings, and has incremental prognostic value (3,4). The coronary artery calcium (CAC) score is a marker of atherosclerotic coronary artery disease and provides incremental predictive value of future cardiovascular events in patients with aortic stenosis (5,6). Mitral annular calcium (MAC) has been identified as an independent predictor of conduction system abnormalities after transcatheter aortic valve replacement (TAVR) (7,8).

Multienergy CT enables material decomposition for separating iodine from calcium. Several previous studies using conventional energy-integrating detector CT (EID-CT) scanners demonstrated the feasibility of virtual noncontrast (VNC) images reconstructed from contrast-enhanced multienergy CT for quantification of coronary calcifications (9–13). While CAC scores determined from VNC images showed high correlation with values from true noncontrast images, scores from VNC images were systematically lower in these studies (9–13). Another drawback of EID-CT is the need for prospective protocolling as multienergy data are otherwise not available (14) except for the dual-layer multienergy technique when performing scans at an appropriate tube potential (9,10).

Recently introduced photon-counting detector CT (PCD-CT) has inherent spectral capabilities at high temporal resolution (15–18). In PCD-CT, incoming photons are detected and resolved based on their energies in a direct conversion process. The subsequent energy thresholding enables the creation of spectral reconstructions (15–17,19,20). Allmendinger et al (19) showed in a phantom study that virtual removal of calcium from coronary arteries is feasible with PCD-CT using multienergy-based material decomposition into calcium and iodine. Emrich et al (20) suggested that the same algorithm can be applied to remove iodine from contrast-enhanced CT, providing

Abbreviations

AVC = aortic valve calcium, CAC = coronary artery calcium, ECG = electrocardiogram, EID-CT = energy-integrating detector CT, MAC = mitral annular calcium, PCD-CT = photon-counting detector CT, QIR = quantum iterative reconstruction, TAVR = transcatheter aortic valve replacement, VNC = virtual noncontrast

Summary

Virtual noncontrast images from cardiac late enhancement scans acquired using photon-counting detector CT yielded accurate quantification of aortic valve, mitral annular, and coronary artery calcium, enabling patient risk stratification.

Key Points

- In a retrospective study of 90 patients who underwent photon-counting detector CT, cardiac calcium scores were similar between true noncontrast images and virtual noncontrast (VNC) images reconstructed from late enhancement cardiac scans at 80 keV, regardless of quantum iterative reconstruction (QIR) strength, for aortic valve and mitral annular calcium and VNC at 70 keV with QIR 4 for coronary artery calcium (all $P > .05$).
- Agreement between severe aortic stenosis likelihood categories on VNC images at 80 keV ($\kappa = 0.974$) and coronary artery calcification risk categories on VNC images at 70 keV ($\kappa = 0.967$) was excellent compared with categories determined on true noncontrast images.

Keywords

Coronary Arteries, Aortic Valve, Mitral Valve, Aortic Stenosis, Calcifications, Photon-counting Detector CT

calcium-preserving VNC images of the heart and potentially obviating the need for a dedicated noncontrast scan.

The purpose of our study was to assess the accuracy of AVC, MAC, and CAC quantification and risk stratification using VNC images from late enhancement PCD-CT as compared with true noncontrast images.

Materials and Methods

Patients

This retrospective single-center study was conducted at an academic medical center after institutional review board and local ethics committee approval was obtained. All patients provided written informed consent.

Consecutive patients screened for TAVR planning with a PCD-CT scan between January and September 2022 were identified. Patients were excluded when raw data of the scans were missing or if severe artifacts compromised image quality (Fig 1).

CT Data Acquisition

All patients underwent scans with a first-generation dual-source PCD-CT system (NAEOTOM Alpha; version syngo CT VA50; Siemens Healthcare) equipped with two cadmium telluride detectors. No β-blockers were administered for heart rate control. The protocol comprised an electrocardiogram (ECG)-gated true noncontrast cardiac scan for calcium scoring followed by ECG-gated coronary CT angiographic and CT aortographic imaging. An ECG-gated late enhancement cardiac scan was acquired 5 minutes after contrast medium injection to assess myocardial fibrosis and to screen for prior myocardial infarcts. Contrast enhancement was achieved by injecting a weight-based volume of iodinated contrast medium (60–80 mL, iopromide, Ultravist 370 mg I/mL; Bayer Healthcare) accompanied by a saline chaser (20 mL, NaCl 0.9%) into an antecubital vein applying a weight-based flow rate (3.3–4.4 mL/sec) (Table S1).

True noncontrast and late enhancement cardiac scans were acquired in the ECG-gated sequential multienergy QuantumPlus mode with prospective gating at an absolute interval of 280 msec from the R wave. Tube potential was set to 120 kV, collimation was 144 × 0.4 mm, and image quality level was set to 20 and 80 for the true noncontrast and late enhancement scan, respectively. Mean volume CT dose index was 3.2 mGy ± 1.2 (SD) for the true noncontrast scan and 7.8 mGy ± 2.8 for the late enhancement scan. The gantry rotation time was 0.25 second for all scans. CT aortographic images were acquired at a tube potential of 120 kV, an image quality level of 64, and a collimation of 144 × 0.4 mm. Scan acquisition and scan dose parameters of ECG-gated coronary CT angiography are provided in Table S2. Because these image data were not used in this study, no further details on reconstruction parameters are provided.

Image Reconstruction and Calcium Scoring

True noncontrast cardiac scans were reconstructed as virtual monoenergetic images at 70 keV without quantum iterative reconstruction (QIR) and served as the reference standard (21–23). In previous phantom studies, CAC quantification was most accurate using virtual monoenergetic images reconstructed with these parameters when compared with conventional EID-CT images without the need of a conversion factor (21–23).

Late enhancement cardiac scans were reconstructed by applying the spectral calcium-preserving virtual noncontrast algorithm (PureCalcium; Siemens Healthineers) (20). In brief, this algorithm performs a series of two-material decompositions and denoising using QIR to generate virtual monoenergetic images in a way that the contrast of voxels containing only calcium is preserved for the targeted image while the iodine signal is subtracted. VNC images were reconstructed at 60, 70, 80, and 90 keV, respectively, applying QIR with strengths of 2, 3, and 4, respectively. Since virtual monoenergetic images of true noncontrast cardiac scans provided the most accurate calcium quantification results at 70 keV compared with EID-CT images (21), VNC images were also reconstructed at 70 keV, as well as at 60, 80, and 90 keV, to assess the influence of different monoenergetic levels on quantification accuracy.

A section thickness of 3 mm, an increment of 1.5 mm, a matrix size of 512 × 512 pixels, and the Qr36 kernel was used for all images. The field of view was set to 200 × 200 mm^2 and was matched between true noncontrast and late enhancement scans.

AVC, MAC, and CAC were quantified using a dedicated, commercially available software (CaScore, syngo.via VB60; Siemens Healthineers) in accordance with the Agatston method (24). The software highlights cardiac calcifications, which were subsequently assigned to a cardiac structure by a reader (S.G.,

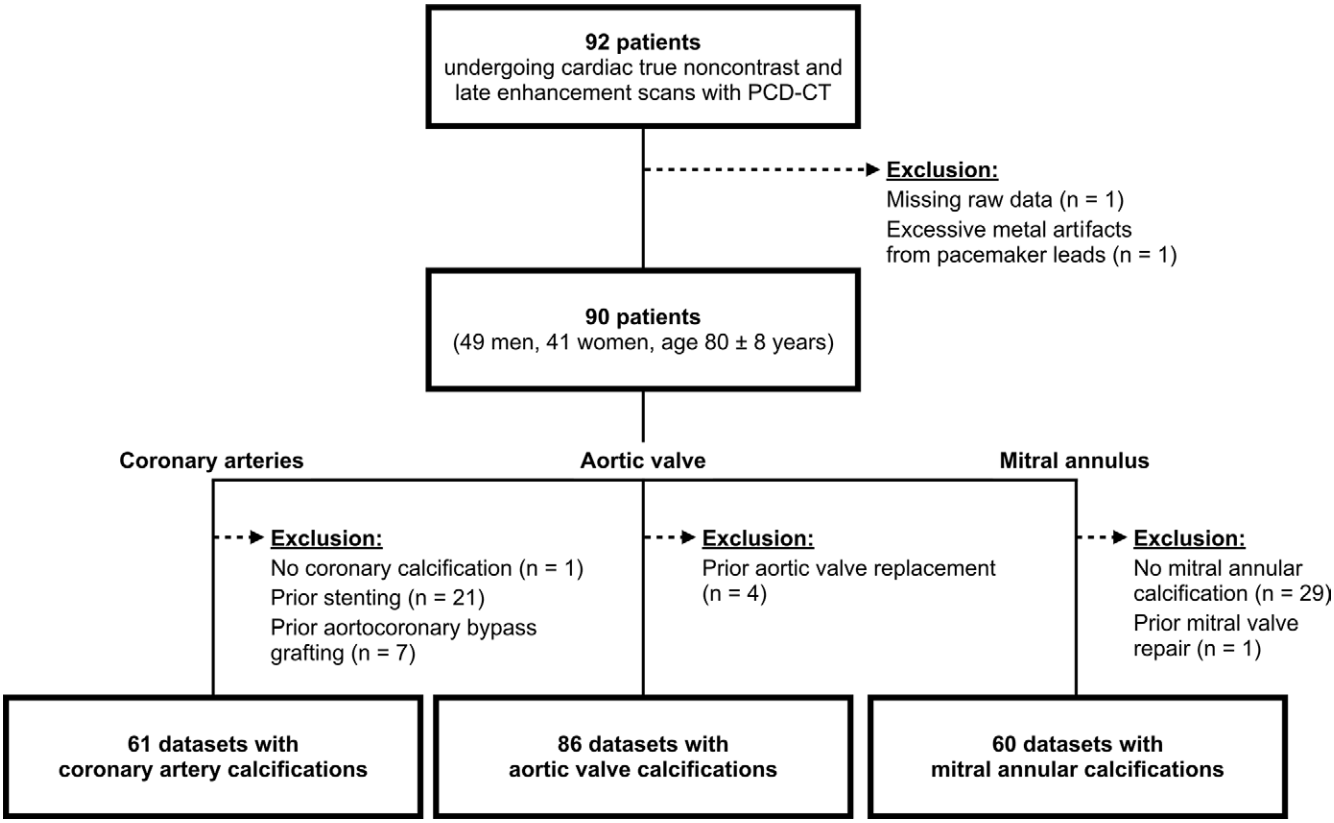

Figure 1: Flowchart details patient inclusion. PCD-CT = photon-counting detector CT.

a medical student). For extensive calcifications associated with more than one cardiac structure, manual adjustments were made by the reader in an identical manner for all image sets of the same patient and reviewed by an expert (V.M., in training with 4 years of experience in cardiovascular radiology). Total calcium scores and volumes for the aortic valve, mitral annulus, and coronary arteries were extracted for every reconstruction. Valves with prior surgery or intervention and coronary arteries with stents or aortocoronary bypass grafting were not considered for analyses since foreign material may impede accurate calcium quantification.

Likelihood of Severe Aortic Stenosis and CAC Risk Categories

AVC scores were subclassified into four categories with regard to the likelihood of severe aortic stenosis: *(a)* highly likely with a score greater than or equal to 1600 for women and greater than or equal to 3000 for men, *(b)* likely with a score greater than or equal to 1200 for women and greater than or equal to 2000 for men, and *(c)* unlikely with a score less than 800 for women and less than 1600 for men (25). According to Hecht et al (26), CAC scores were stratified into four risk categories defined by the following score boundaries: 0, 1–99, 100–299, and greater than 300. In addition, a binary CAC score for risk prediction of short-term mortality after TAVR was used with a threshold score of 1000 (6).

Statistical Analysis

Analyses were performed using R statistical software (R, version 4.2.1; R Foundation, *https://www.R-project.org/*). The Shapiro-Wilk test was used to test variables for normal distribution. Variables are presented as means ± SDs when normally distributed and as medians and interquartile ranges when nonnormally distributed. Categorical variables are reported as counts and percentages. Calcium scores and volumes determined on VNC images and the reference standard were compared using Bland-Altman analyses, linear regression models, two-way intraclass correlation coefficient (from 0 to 1.00, with 0.81–1.00 indicating excellent agreement), and Wilcoxon signed rank tests. *P* values were adjusted with the Benjamini-Hochberg procedure for multiple comparisons. A two-tailed *P* value less than .05 was considered to indicate statistical significance. Agreement between risk categories determined with VNC findings and the reference standard was assessed by weighted κ analysis (from 0 to 1.00, with 0.81–1.00 indicating excellent agreement).

Results

Patient Characteristics

Of 92 eligible patients, one patient was excluded because of missing raw data and one patient was excluded because of severe artifacts from pacemaker leads compromising image quality. No patient had to be excluded because of motion artifacts. A total of 90 patients (41 female patients, 49 male patients; mean age, 80 years ± 8; body mass index, 26 kg/m^2 ± 5) were finally included. For analyses, exclusions were as follows: four patients for aortic valves with prior valve replace-

ment, 29 patients for mitral annuli that had no calcifications, one patient for mitral annulus with prior mitral valve repair, one patient for having no coronary artery calcification, 21 patients for having coronary stents, and seven patients for having aortocoronary bypass grafts. Finally, 86 aortic valve, 60 mitral annular, and 61 coronary artery calcifications were evaluated (see Fig 1). Baseline characteristics and CT radiation dose metrics are detailed in Table 1. Table S3 provides information on aortic valve disease, including type of valve disease, echocardiographic findings, and treatment. Figure 2 and Figure 3 provide representative examples of the reconstructions.

Table 1: Patient Baseline Characteristics

Patient Characteristic	All Patients (n = 90)
Sex	
Male patients	49 (54)
Female patients	41 (46)
Age (y)	80 ± 8 (range, 56–96)
Body mass index (kg/m^2)	26.1 ± 4.8 (range, 15.9–49.7)
Heart rate during the scans (beats/min)	
True noncontrast scans*	71 (IQR, 65–84)
Late enhancement scans*	68 (IQR, 61–82)
Medical history	
Hypertension	68/90 (76)
Dyslipidemia	44/90 (49)
Diabetes	29/90 (32)
Smoking	33/90 (37)
Chronic obstructive pulmonary disease	8/90 (9)
Chronic kidney disease	33/90 (37)
CT radiation dose	
True noncontrast scan	
Volume CT dose index (mGy)	3.2 ± 1.2 (range, 1.6–8.1)
Dose length product (mGy · cm)	48.2 ± 16.7 (range, 24.4–108.0)
Late enhancement scan	
Volume CT dose index (mGy)	7.9 ± 2.7 (range, 3.9–18.0)
Dose length product (mGy · cm)	110.5 ± 36.5 (range, 54.2–238.0)

Note.—Unless otherwise specified, data are means ± SDs or proportion of patients with percentages in parentheses.
* Data are medians, with IQRs in parentheses.

Calcium Score Quantification

Median scores determined on true noncontrast images were 2287 (IQR, 1570–3359) for AVC, 998 (IQR, 247–3209) for MAC, and 571 (IQR, 135–1799) for CAC (Table S4).

AVC scores on VNC images at 80 keV with QIR 4 revealed the smallest difference (mean difference, 3; limits of agreement, -357, 363), strong correlation (r = 0.98), and excellent agreement (intraclass correlation coefficient, 0.992) compared with AVC scores on true noncontrast images (Table 2 and Fig 4). Regardless of the QIR strength, AVC scores determined on VNC images at 80 keV were similar to the reference standard (QIR 2–4; all P > .05) and showed significant differences on all VNC images at 60, 70, and 90 keV (QIR 2–4; all P < .001).

MAC scores on VNC images at 80 keV with QIR 4 revealed the smallest difference (mean difference, 6; limits of agreement, -50, 62), strong correlation (r = 0.99), and excellent agreement (intraclass correlation coefficient, 0.997) compared with MAC scores on true noncontrast images. MAC scores were similar to the reference standard on VNC images at 80 keV regardless of the QIR strength (QIR 2–4; all P > .05) and differed significantly on all VNC images at 60, 70, and 90 keV (QIR 2–4, all P < .001).

CAC scores on VNC images at 70 keV with QIR 4 revealed the smallest difference (mean difference, 28; limits of agreement, -214, 269), strong correlation (r = 0.99), and excellent agreement (intraclass correlation coefficient, 0.996) compared with CAC scores on true noncontrast images. CAC scores determined on VNC images at 70 keV with QIR 4 were similar to the reference standard (P = .05) and differed significantly on VNC images at 70 keV with QIR 2 (P = .02) or QIR 3 (P = .04) and on all VNC images at 60, 80, or 90 keV (QIR 2–4; all P < .001). No patient with CAC (score > 0) determined on true noncontrast images had a score of 0 on VNC images. Results of calcium scores are presented in detail in Table 2 and Table S4. Results of calcium volumes are presented in Table S5, Table S6, and Figure S1.

Likelihood of Severe Aortic Stenosis

AVC of 41 female and 45 male patients were evaluated. Based on the AVC scores determined on true noncontrast images, severe aortic stenosis was highly likely in 28 female patients (score ≥ 1600) and 20 male patients (score ≥ 3000), likely in four female patients (score ≥ 1200) and nine male patients (score ≥ 2000), and unlikely in five female patients (score < 800) and 10 male patients (score < 1600). Scores ranged between 800 and 1200 in four female patients and between 1600 and 2000 in six male patients. Agreement of likelihood categories was lowest for VNC images at 60 keV (QIR 2–4) (κ = 0.857 for all) with a concordance of 74% (64 of 86 patients) (Table S7). Agreement of likelihood categories was highest for VNC images at 80 keV with QIR 2 or 3 (κ = 0.974 for both) with a concordance of 93% (80 of 86 patients). Using VNC images at 80 keV with QIR 2 or 3, likelihood categories were overestimated in four of 86 patients (5%) and underestimated in two of 86 patients (2%) (Fig 5).

CAC Risk Categories

CAC scores determined on true noncontrast images ranged between 0 and 99 in seven patients, between 100 and 299 in 13 patients, and were over 300 in 41 patients. Agreement of risk categories was lowest for VNC images at 90 keV with QIR 4 (κ = 0.788), and agreement was highest for VNC images at 70 keV, regardless of the QIR strength (all κ = 0.967) (Table

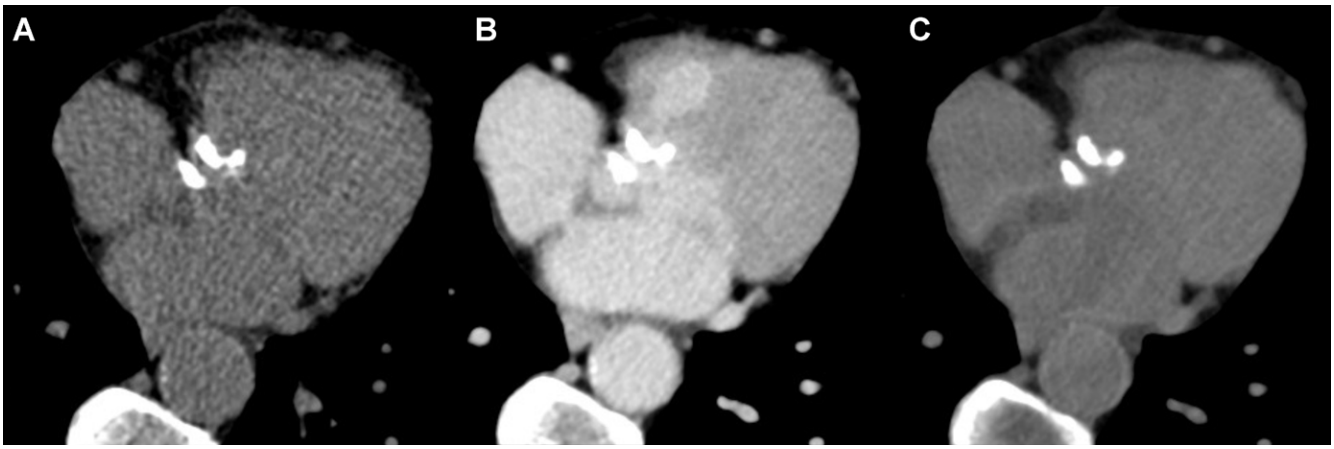

Figure 2: Representative CT images with aortic valve calcifications. Axial CT images in a 75-year-old female patient with severe aortic stenosis show **(A)** true noncontrast (at 70 keV without quantum iterative reconstruction [QIR]), **(B)** late enhancement (at 55 keV with QIR 3), and **(C)** virtual noncontrast (at 80 keV with QIR 3). Volume CT dose index of the true noncontrast and late enhancement scans were 1.9 mGy and 4.6 mGy, respectively. The aortic valve calcium scores were 2053 on true noncontrast images and 2051 on virtual noncontrast images (at 80 keV with QIR 4).

Figure 3: Representative CT images with coronary artery calcifications. Axial CT images in an 81-year-old female patient with severe aortic stenosis show **(A)** true noncontrast (at 70 keV without quantum iterative reconstruction [QIR]), **(B)** late enhancement (at 55 keV with QIR 4), and **(C)** virtual noncontrast (at 70 keV with QIR 4). Volume CT dose index of the true noncontrast and the late enhancement scans were 2.6 mGy and 6.3 mGy, respectively. The coronary artery calcium scores were 1336 on true noncontrast images and 1411 on virtual noncontrast images (70 keV with QIR 4). Note that small calcifications in the aortic root were removed on virtual noncontrast images, while coronary calcifications appear similar on true noncontrast and virtual noncontrast images.

S7). Concordance of CAC risk categories was 97% (59 of 61 patients) when using VNC images at 70 keV (QIR 2–4), while two patients were reclassified to lower risk categories (Fig 5).

Binary CAC stratification for predicting short-term mortality in patients undergoing TAVR revealed CAC scores less than 1000 in 40 patients and greater than or equal to 1000 in 21 patients. Concordance was very high regardless of the virtual monoenergetic level and QIR strength of VNC images (all 100%).

Discussion

In patients with aortic stenosis, accurate quantification of aortic valve, mitral annular, and coronary artery calcifications on noncontrast cardiac CT images is important for risk stratification (3–8). PCD-CT enables the reconstruction of VNC images from contrast-enhanced images through multienergy-based material decomposition, potentially obviating the need of acquiring a separate noncontrast scan. The present study indicates that calcium quantification using VNC images from PCD-CT yields similar results as compared with true noncontrast images when VNC images at 80 keV are used for AVC and MAC scores, regardless of the QIR strength, and when VNC images at 70 keV with QIR 4 are used for measuring CAC (all $P > .05$). Importantly, agreement between categories was excellent when assessing the likelihood of severe aortic stenosis on VNC images at 80 keV ($\kappa = 0.974$) and when determining CAC risk categories on VNC images at 70 keV ($\kappa = 0.967$). Binary CAC stratification using VNC images, regardless of QIR strength, had very high concordance (100%) with the reference standard.

In this study, we used VNC images from cardiac late enhancement PCD-CT in patients screened for TAVR planning. Late enhancement scans are powerful for quantifying myocardial fibrosis and detecting cardiac amyloidosis, which both substantially impact patient prognosis after TAVR (27–29).

Emrich et al (20) were the first to describe the calcium-preserving VNC algorithm for PCD-CT data and compared CAC

Table 2: Comparison of Cardiac Calcium Score Quantification

keV and QIR	Aortic Valve Calcium					Mitral Annular Calcium					Coronary Artery Calcium				
	Difference*	LoA	*P* Value	*r* Value	ICC	Difference*	LoA	*P* Value	*r* Value	ICC	Difference*	LoA	*P* Value	*r* Value	ICC
60															
2	588 (518, 659)	−59, 1236	<.001	0.98	0.977	419 (299, 539)	−492, 1329	<.001	1	0.989	219 (155, 284)	−273, 712	<.001	0.99	0.985
3	609 (536, 682)	−57, 1275	<.001	0.98	0.976	433 (309, 556)	−505, 1370	<.001	1	0.989	238 (175, 302)	−249, 725	<.001	0.99	0.986
4	622 (548, 696)	−55, 1299	<.001	0.98	0.975	432 (303, 561)	−545, 1410	<.001	1	0.988	245 (175, 314)	−284, 773	<.001	0.99	0.983
70															
2	258 (209, 306)	−187, 702	<.001	0.98	0.988	189 (117, 262)	−363, 742	<.001	1	0.996	34 (3, 65)	−205, 273	.02	0.99	0.996
3	264 (215, 313)	−186, 714	<.001	0.98	0.988	196 (121, 271)	−370, 762	<.001	1	0.996	31 (0, 62)	−206, 267	.04	0.99	0.996
4	267 (218, 317)	−186, 721	<.001	0.98	0.988	198 (122, 274)	−380, 775	<.001	1	0.995	28 (−4, 59)	−214, 269	.05	0.99	0.996
80															
2	11 (−29, 50)	−347, 369	.51	0.98	0.992	13 (−40, 66)	−388, 414	.95	1	0.998	−118 (−164, −72)	−468, 232	<.001	0.99	0.991
3	8 (−31, 46)	−343, 359	.51	0.98	0.992	16 (−38, 69)	−388, 420	.95	1	0.998	−111 (−151, −70)	−423, 201	<.001	0.99	0.993
4	3 (−36, 43)	−357, 363	.35	0.98	0.992	6 (−50, 62)	−420, 432	.95	0.99	0.997	−121 (−166, −76)	−467, 224	<.001	0.99	0.991
90															
2	−193 (−233, −154)	−552, 165	<.001	0.98	0.991	−154 (−234, −74)	−761, 453	<.001	0.99	0.994	−223 (−290, −156)	−731, 284	<.001	0.99	0.977
3	−202 (−241, −162)	−563, 159	<.001	0.98	0.991	−161 (−238, −83)	−749, 428	<.001	0.99	0.995	−229 (−297, −161)	−744, 287	<.001	0.99	0.976
4	−208 (−248, −168)	−571, 154	<.001	0.98	0.991	−166 (−244, −88)	−757, 425	<.001	0.99	0.995	−235 (−303, −166)	−751, 282	<.001	0.99	0.976

Note.— ICC = intraclass correlation coefficient, keV = kiloelectron volt, LoA = limits of agreement, QIR = quantum iterative reconstruction.
* Data in parentheses are 95% CIs.

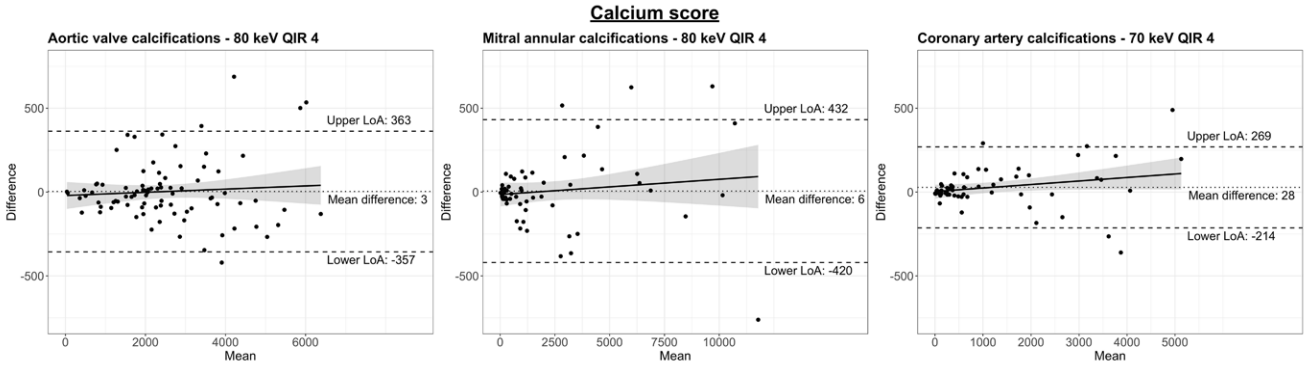

Figure 4: Bland-Altman plots comparing calcium scores of **(A)** the aortic valve, **(B)** the mitral annulus, and **(C)** the coronary arteries determined on true noncontrast images and virtual noncontrast images. Results of the virtual noncontrast images with the smallest differences are presented depending on the cardiac structure under study. Note that differences are smaller at lower scores and greater when more extensive calcifications are present. The dotted line indicates the mean difference, and the dashed lines indicate the lower and upper limits of agreement. The solid line corresponds to a regression line, and the shaded areas indicate the 95% CIs for the regression line. LoA = limit of agreement, QIR = quantum iterative reconstruction.

scores determined on VNC images from coronary CT angiography at 70 keV using QIR 2 with CAC scores determined on true noncontrast images. Their results showed a significant underestimation of CAC scores on VNC images (mean difference of -114). In contrast to Emrich et al (20), our study concept was to replace the true noncontrast scan for calcium quantification with VNC images from late enhancement PCD-CT. Iodine mapping for quantifying myocardial fibrosis and amyloidosis in patients with severe aortic stenosis can be performed from the same image data set that can also be used for generating VNC images for calcium quantification. We found that CAC scores determined on VNC images at 70 keV using QIR 4 were comparable with CAC scores determined on true noncontrast images (mean difference, 28; $P = .05$), providing more accurate values than those described in the study by Emrich et al (20). Differences in the results may be related to the higher CAC score in our study (median, 571 vs 232 in the study by Emrich et al [20]). Accurate CAC scoring may be more challenging in patients with lower scores because plaques with low attenuation or small volumes could be more difficult to detect on spectral images. Identifying the type of calcifications that are susceptible to higher quantification variability or defective appearance on VNC images continues to be the subject of research. Nevertheless, results of this study show that calcium quantification on VNC images is accurate for large, round-shaped calcifications such as AVC, crescent-shaped calcifications such as MAC, and smaller, linear calcifications such as CAC. Another reason for the discrepancy might be the newer software version used in our study (syngo CT VA50) compared with that used by Emrich et al (syngo CT VA40) (20). According to the vendor, the newer software improved the spectral image quality and material decomposition, which might have impacted our study results. Finally, the lower attenuation of the blood pool on late enhancement images compared with coronary CT angiographic images may have also contributed to a more accurate material decomposition in our study. Collectively, our study suggests that VNC images are a valuable substitute for true noncontrast images and offer the possibility of accurate cardiac calcium quantification in routine clinical practice. Though, performing a late enhancement scan in patients screened for TAVR planning may not yet be routine in many centers.

In contrast to CAC scores, AVC and MAC scores on VNC images at 70 keV showed a systematic overestimation of calcification scores. A possible speculative explanation for this finding could be that residual iodine in the center of macrocalcifications was not entirely subtracted by the VNC algorithm, and iodine-containing voxels were subsequently erroneously added to the true calcium voxels due to the simple voxel counting algorithm underlying the Agatston score (24). Considering the VNC algorithm, this shortcoming may be attributed to a limitation in the combined spectral and spatial resolution. Our data indicate that this limitation can be overcome by using VNC images at 80 keV for AVC and MAC scoring. The suggested switch to VNC images at 80 keV for AVC or MAC does not change the iodine contribution to the score as such but leads to a downgrading of the total score by a few percentage points due to the weighing dependency of the Agatston score on the maximum realized attenuation of the evaluated lesion. Choosing higher monoenergetic levels lowers the weighing on average because of the inherent kiloelectron-volts dependency of the score (22).

Application of iterative reconstruction algorithms on noncontrast images acquired using EID-CT may lead to an underestimation of AVC and CAC scores, thus impairing risk stratification (30,31). With PCD-CT, calcium quantification on VNC images was not influenced by the QIR strengths for AVC and MAC, whereas CAC scores on VNC images differed from the reference standard depending on QIR strengths, however, without a clear trend.

In our study, true noncontrast scans for calcium scoring were acquired with an image quality level of 20, resulting in a mean volume CT dose index of 3.2 mGy. In comparison, cardiac late enhancement scans were acquired with a higher image quality level of 80 to ensure a sufficient quality for spectral reconstructions with iodine mapping in the myocardium (mean volume CT dose index, 7.9 mGy). However, since calcium scoring on VNC images from PCD-CT was accurate, late enhancement

scans may replace separate true noncontrast scans in the future.

The following study limitations merit consideration. First, this retrospective, single-center study included a limited number of patients. Second, true noncontrast and late enhancement scans were not acquired with the same image quality level. However, a previous phantom study found no evidence that CAC scoring was dependent on the chosen image quality level (21). Third, heart rates during scan acquisition were relatively high (ie, median, 71 beats per minute during true noncontrast scans; median, 68 beats per minute during late enhancement scans). Lower heart rates may lead to more accurate calcium quantification on both true noncontrast images and VNC images. Fourth, both true noncontrast and late enhancement cardiac scans were acquired in the ECG-gated sequential mode. Further studies are needed to evaluate the consistency of VNC performance in scans acquired in the helical mode. Fifth, minor discrepancies between calcium quantification on VNC and true noncontrast images may be present due to divergent segmentation of extensive calcifications. Certainly, every effort was made to perform identical segmentation on all reconstructions, and manual adjustments were only necessary in a minority of patients. Sixth, cardiac calcifications were evaluated on VNC images reconstructed at only four different monoenergetic levels. Using these reconstructions, calcium quantification yielded accurate results and also over- and underestimated results when compared with the reference standard for all cardiac structures studied. Therefore, the inclusion of even lower or higher monoenergetic levels would not further strengthen our results. Finally, the potential impact of reclassification based on calcium quantification using VNC images on outcome predictions was not evaluated.

In conclusion, VNC images from cardiac PCD-CT enabled accurate calcium quantification and risk stratification of aortic, mitral annular, and coronary artery calcifications. Future studies should evaluate the prognostic value of calcium quantification using VNC images.

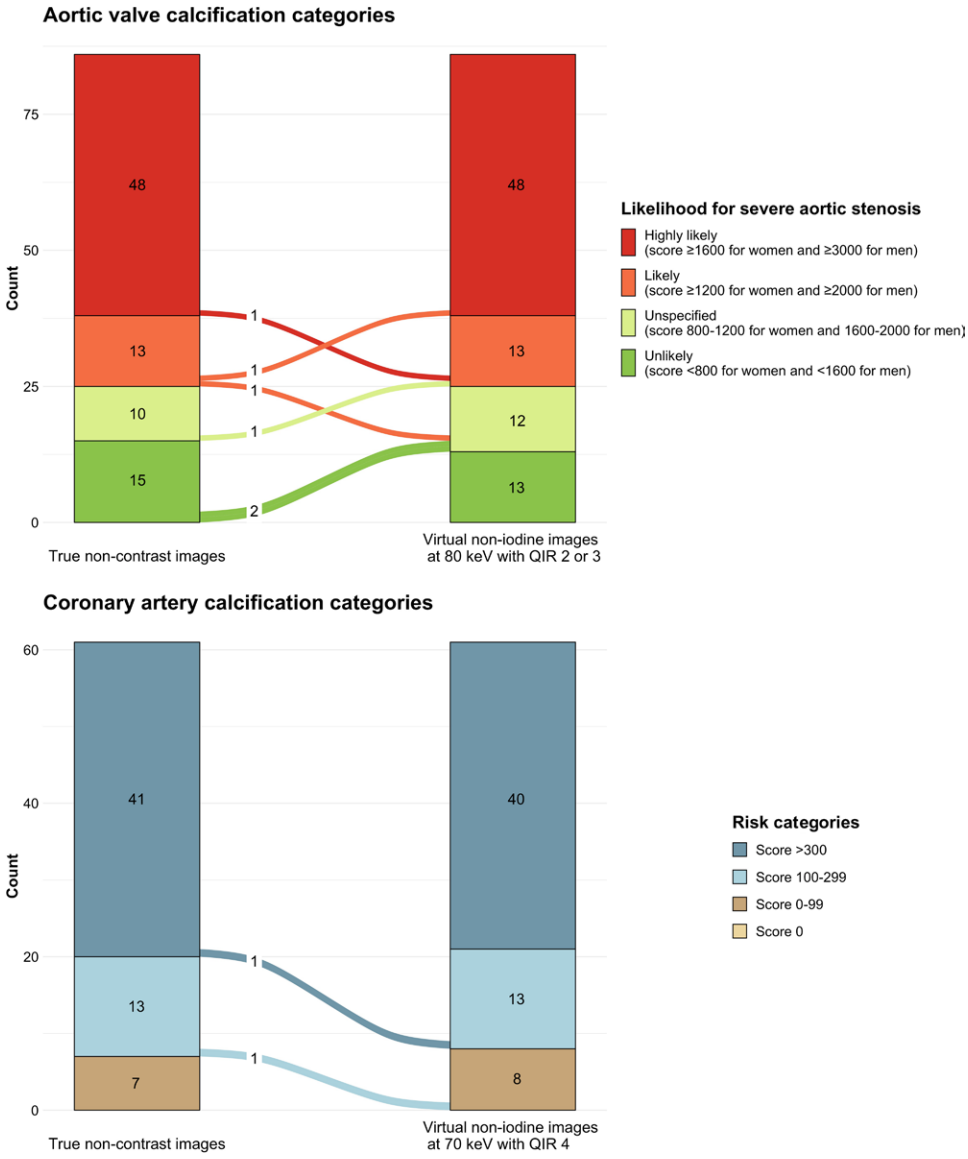

Figure 5: Diagram illustrates the concordance and discordance of **(A)** aortic valve calcium and **(B)** coronary artery calcium categories using scores determined on virtual noncontrast (VNC) images compared with true noncontrast images. Severe aortic stenosis likelihood categories **(A)** on VNC images at 80 keV with QIR 2 or 3 showed excellent agreement (κ = 0.974; concordance of 93% in 80 of 86 patients) with categories determined using true noncontrast images. Likelihood categories were overestimated in four of 86 (5%) and underestimated in two of 86 reclassified patients (2%). CAC risk categories **(B)** on VNC images at 70 keV with QIR 4 showed excellent agreement (κ = 0.967) with categories determined using true noncontrast images. Concordance of CAC risk categories was 97% (59 of 61 patients), while two patients were reclassified to lower risk categories. QIR = quantum iterative reconstruction.

Author contributions: Guarantors of integrity of entire study, **V.M.**, **H.A.**, **M.E.**; study concepts/study design or data acquisition or data analysis/interpretation, all authors; manuscript drafting or manuscript revision for important intellectual content, all authors; approval of final version of submitted manuscript, all authors; agrees to ensure any questions related to the work are appropriately resolved, all authors; literature research, **V.M.**, **S.G.**, **R.M.**, **A.M.K.**, **H.A.**, **M.E.**; clinical studies, **V.M.**, **S.G.**, **T.S.**, **A.M.K.**, **H.A.**, **M.E.**; statistical analysis, **V.M.**, **S.G.**, **T.S.**, **R.M.**, **H.A.**, **M.E.**; and manuscript editing, all authors

Data sharing: Data generated or analyzed during the study are available from the corresponding author by request.

Disclosures of conflicts of interest: **V.M.** No relevant relationships. **S.G.** No relevant relationships. **T.S.** No relevant relationships. **R.M.** Speaker fees from Siemens and Bayer. **A.E.** No relevant relationships. **A.M.K.** No relevant relationships. **H.A.**

Member of Siemens speakers bureau; institutional grants from Bayer, Canon, Guerbet, and Siemens. **M.E.** Speaker fee from Siemens.

References

1. Shekar C, Budoff M. Calcification of the heart: mechanisms and therapeutic avenues. Expert Rev Cardiovasc Ther 2018;16(7):527–536.
2. Abbara S, Blanke P, Maroules CD, et al. SCCT guidelines for the performance and acquisition of coronary computed tomographic angiography: A report of the society of Cardiovascular Computed Tomography Guidelines Committee: Endorsed by the North American Society for Cardiovascular Imaging (NASCI). J Cardiovasc Comput Tomogr 2016;10(6):435–449.
3. Christensen JL, Tan S, Chung HE, et al. Aortic valve calcification predicts all-cause mortality independent of coronary calcification and severe stenosis. Atherosclerosis 2020;307:16–20.
4. Pawade T, Clavel MA, Tribouilloy C, et al. Computed Tomography Aortic Valve Calcium Scoring in Patients With Aortic Stenosis. Circ Cardiovasc Imaging 2018;11(3):e007146.
5. Erbel R, Möhlenkamp S, Moebus S, et al. Coronary risk stratification, discrimination, and reclassification improvement based on quantification of subclinical coronary atherosclerosis: the Heinz Nixdorf Recall study. J Am Coll Cardiol 2010;56(17):1397–1406.
6. Eberhard M, Hinzpeter R, Schönenberger ALN, et al. Incremental Prognostic Value of Coronary Artery Calcium Score for Predicting All-Cause Mortality after Transcatheter Aortic Valve Replacement. Radiology 2021;301(1):105–112.
7. Brodov Y, Konen E, Di Segni M, et al. Mitral Annulus Calcium Score. Circ Cardiovasc Imaging 2019;12(1):e007508.
8. Okuno T, Brugger N, Asami M, et al. Clinical impact of mitral calcium volume in patients undergoing transcatheter aortic valve implantation. J Cardiovasc Comput Tomogr 2021;15(4):356–365.
9. Gassert FG, Schacky CE, Müller-Leisse C, et al. Calcium scoring using virtual non-contrast images from a dual-layer spectral detector CT: comparison to true non-contrast data and evaluation of proportionality factor in a large patient collective. Eur Radiol 2021;31(8):6193–6199.
10. Nadjiri J, Kaissis G, Meurer F, et al. Accuracy of Calcium Scoring calculated from contrast-enhanced Coronary Computed Tomography Angiography using a dual-layer spectral CT: A comparison of Calcium Scoring from real and virtual non-contrast data. PLoS One 2018;13(12):e0208588.
11. Song I, Yi JG, Park JH, Kim SM, Lee KS, Chung MJ. Virtual Non-Contrast CT Using Dual-Energy Spectral CT: Feasibility of Coronary Artery Calcium Scoring. Korean J Radiol 2016;17(3):321–329.
12. Schwarz F, Nance JW Jr, Ruzsics B, Bastarrika G, Sterzik A, Schoepf UJ. Quantification of coronary artery calcium on the basis of dual-energy coronary CT angiography. Radiology 2012;264(3):700–707.
13. Yamada Y, Jinzaki M, Okamura T, et al. Feasibility of coronary artery calcium scoring on virtual unenhanced images derived from single-source fast kVp-switching dual-energy coronary CT angiography. J Cardiovasc Comput Tomogr 2014;8(5):391–400.
14. Rajiah P, Parakh A, Kay F, Baruah D, Kambadakone AR, Leng S. Update on Multienergy CT: Physics, Principles, and Applications. RadioGraphics 2020;40(5):1284–1308.
15. Flohr T, Petersilka M, Henning A, Ulzheimer S, Ferda J, Schmidt B. Photon-counting CT review. Phys Med 2020;79:126–136.
16. Mergen V, Sartoretti T, Klotz E, et al. Extracellular Volume Quantification With Cardiac Late Enhancement Scanning Using Dual-Source Photon-Counting Detector CT. Invest Radiol 2022;57(6):406–411.
17. Si-Mohamed SA, Boccalini S, Lacombe H, et al. Coronary CT Angiography with Photon-counting CT: First-In-Human Results. Radiology 2022;303(2):303–313.
18. Rajagopal JR, Farhadi F, Richards T, et al. Evaluation of Coronary Plaques and Stents with Conventional and Photon-counting CT: Benefits of High-Resolution Photon-counting CT. Radiol Cardiothorac Imaging 2021;3(5):e210102.
19. Allmendinger T, Nowak T, Flohr T, et al. Photon-Counting Detector CT-Based Vascular Calcium Removal Algorithm: Assessment Using a Cardiac Motion Phantom. Invest Radiol 2022;57(6):399–405.
20. Emrich T, Aquino G, Schoepf UJ, et al. Coronary Computed Tomography Angiography-Based Calcium Scoring: In Vitro and In Vivo Validation of a Novel Virtual Noniodine Reconstruction Algorithm on a Clinical, First-Generation Dual-Source Photon Counting-Detector System. Invest Radiol 2022;57(8):536–543.
21. Eberhard M, Mergen V, Higashigaito K, et al. Coronary Calcium Scoring with First Generation Dual-Source Photon-Counting CT-First Evidence from Phantom and In-Vivo Scans. Diagnostics (Basel) 2021;11(9):1708.
22. van der Werf NR, Greuter MJW, Booij R, van der Lugt A, Budde RPJ, van Straten M. Coronary calcium scores on dual-source photon-counting computed tomography: an adapted Agatston methodology aimed at radiation dose reduction. Eur Radiol 2022;32(8):5201–5209.
23. van der Werf NR, Booij R, Greuter MJW, et al. Reproducibility of coronary artery calcium quantification on dual-source CT and dual-source photon-counting CT: a dynamic phantom study. Int J Cardiovasc Imaging 2022;38(7):1613–1619.
24. Agatston AS, Janowitz WR, Hildner FJ, Zusmer NR, Viamonte M Jr, Detrano R. Quantification of coronary artery calcium using ultrafast computed tomography. J Am Coll Cardiol 1990;15(4):827–832.
25. Baumgartner H, Falk V, Bax JJ, et al. 2017 ESC/EACTS Guidelines for the management of valvular heart disease. Eur Heart J 2017;38(36):2739–2791.
26. Hecht HS, Blaha MJ, Kazerooni EA, et al. CAC-DRS: coronary artery calcium data and reporting system. An expert consensus document of the society of cardiovascular computed tomography (SCCT). J Cardiovasc Comput Tomogr 2018;12(3):185–191.
27. Scully PR, Patel KP, Saberwal B, et al. Identifying Cardiac Amyloid in Aortic Stenosis: ECV Quantification by CT in TAVR Patients. JACC Cardiovasc Imaging 2020;13(10):2177–2189.
28. Everett RJ, Treibel TA, Fukui M, et al. Extracellular Myocardial Volume in Patients With Aortic Stenosis. J Am Coll Cardiol 2020;75(3):304–316.
29. Nitsche C, Scully PR, Patel KP, et al. Prevalence and Outcomes of Concomitant Aortic Stenosis and Cardiac Amyloidosis. J Am Coll Cardiol 2021;77(2):128–139.
30. Caruso D, De Cecco CN, Schoepf UJ, et al. Correction Factors for CT Coronary Artery Calcium Scoring Using Advanced Modeled Iterative Reconstruction Instead of Filtered Back Projection. Acad Radiol 2016;23(12):1480–1489.
31. Hinzpeter R, Weber L, Euler A, et al. Aortic valve calcification scoring with computed tomography: impact of iterative reconstruction techniques. Int J Cardiovasc Imaging 2020;36(8):1575–1581.